

LASER MELTING OF Ti-Ni SHAPE MEMORY ALLOY

H. Kyogoku*, J.A. Ramos** and D.L. Bourell***

*Department of Mechanical Engineering, Kinki University,
Higashihiroshima, Hiroshima 739-2116 Japan

**Department of Mechanical Engineering and Metallurgy, Pontificia Universidad Católica de
Chile, Av. Vicuña Mackenna 4860, Santiago, Chile

***Department of Mechanical Engineering, The University of Texas at Austin,
Austin, TX 78712

Reviewed, accepted August 28, 2003

Abstract

The applicability of laser melting in fabrication of Ti-Ni shape memory alloy was investigated experimentally. Elemental powders of Ti and Ni and mechanically alloyed (MA) TiNi powder were used to fabricate specimens. The effects of powder characteristics on the microstructure and shape memory characteristics of the alloy were examined. The morphology and microstructure of the laser-melted specimens were varied with fabrication conditions. Parts fabricated from elemental powders exhibited a shape memory effect, but those from MA powder did not exhibit it, although the latter showed more homogeneous microstructure than the former.

Introduction

Laser sintering or melting is one of the rapid prototyping processes which can produce complex-shape parts directly from metals and ceramics powders, and this process has been applied to fabricate various parts, molds and so on[1-3]. Shape memory alloys, especially Ti-Ni alloys, are widely applied as joints, springs, actuators in the field of industry as well as functional elements in the field of medical, energy industry and so on because they have not only excellent shape memory characteristics but also superior erosion and corrosion resistances. One of the authors has been reported that shape memory alloys fabricated by a pulse-current pressure sintering method have superior thermo-mechanical characteristics[4-6] and high erosion and corrosion resistances[7,8]. However, since the sintering of elementally blended powders resulted in inhomogeneous microstructure in the sintered compacts, it was found that the alloys obtained have some problems in fatigue properties and temperature-response. Also, since it is difficult for the pulse-current pressure sintering technique to fabricate complicated-shape parts, the application of laser sintering or melting to fabrication of shape memory parts is significant. But there have been no reports on the application of this technique to shape memory alloys.

In this study, we attempt to fabricate Ti-Ni shape memory alloys by CO₂ laser melting. The laser melting conditions are investigated experimentally, and the microstructure and shape memory characteristics of the laser-melted specimens are also examined.

Experimental Method

Experimental procedure

In this study, we used a gas-atomized Ti powder and a carbonyl Ni powder. The mean particle diameter and chemical compositions are shown in Table 1. We prepared two types of powders: (1) Ti-50.2at%Ni elementally blended powder and (2) Ti-50.2at%Ni mechanically alloyed (MA) powder. The blended powder of Ti and Ni was prepared by a V-blender at the composition of Ti-50.2at%Ni. The MA powder was fabricated by means of a planetary ball mill. The ball to powder weight ratio was 5:1. The powder mixture of Ti and Ni powders milled together with stainless steel balls in an atmosphere of argon gas at various rotational speed for various milling time between 3.6 ks and 360 ks. In this study, we used the MA powder milled at 500 rpm for 36 ks. The MA powder obtained was in amorphous state judging from the result of

X-ray diffraction patterns as shown in Fig.1. The oxygen and carbon contents of this powder were 0.28 mass% and 0.075 mass%, respectively. These powders were filled into an aluminum die coated with carbon spray and then laser-melted by means of a CO₂ laser equipment.

Table 1 Mean particle diameters and chemical compositions of Ti and Ni powders

| | Powder | Mean particle diameter (μm) | Chemical compositions (mass%) | | | | |
|----|---------------------|--|-------------------------------|-------|-------|-------|-------|
| | | | Fe | O | N | H | C |
| Ti | Gas-atomized powder | 24 | 0.053 | 0.13 | 0.005 | 0.007 | 0.009 |
| Ni | Carbonyl powder | 6.2 | 0.003 | 0.069 | — | — | 0.078 |

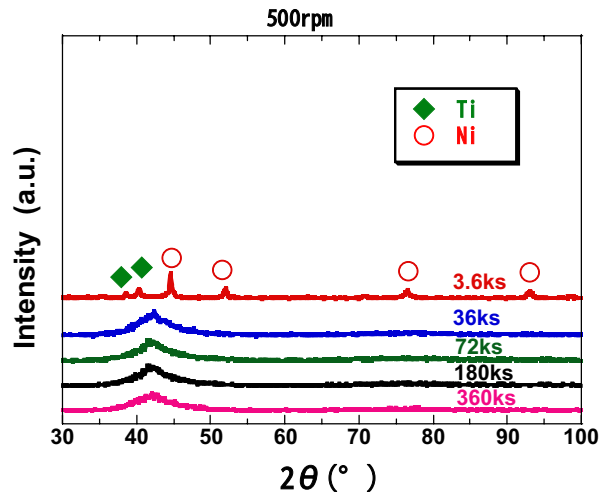


Fig.1 X-ray diffraction patterns of MA powders

The laser melting process scheme consisted of a CO₂ laser beam raster-scanned along a rectangular area, so that a pseudo-energy line source was traversed over a pre-placed powder. The laser beam was focused down a spot of diameter 0.35 mm \pm 0.05mm. By altering the density of scan lines per inch, the width and length of the scan pattern, the scan step and scan period, multiple combinations of scan speed (V_s 508-816 mm/s) and traveling speed (V_t 0.41-3.05 mm/s) were achieved. The laser power delivered at the free surface corresponded to 152-334 W. Fig. 2 shows a schematic diagram of this setup. The powder was compacted manually inside a rectangular trough of dimensions 25.4 mm x 12.7 mm x 6.35 mm carved out in an aluminum holder of dimensions 50.8 mm x 76.2 mm x 25.4 mm and placed inside of the right piston in the CO₂ laser processing chamber. The trough was previously spray-coated with graphite to prevent melting of the aluminum and ease the removal of the cast material. The powder surface was then leveled so that it matched the focal position of the laser beam. The chamber was initially brought to a rough vacuum of approximately 250 mmTorr; the powder was then allowed to degas for 24 hours under a vacuum of 60 mmTorr. During the laser melting, argon gas was purged directly to the processing zone from an annular ring located above the powder bed.

The microstructures of the specimens were examined by optical microscope, scanning electron microscope with EDX and X-ray diffractometer. The shape memory characteristics were examined by DSC equipment.

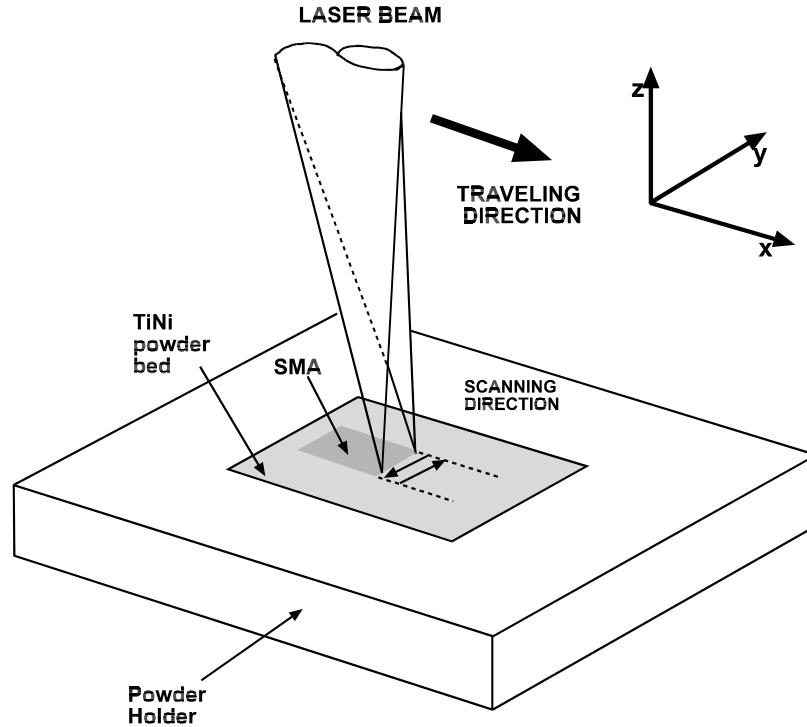


Fig. 2 Schematic diagram of the laser melting of a shape memory alloy powder.

Results and Discussions

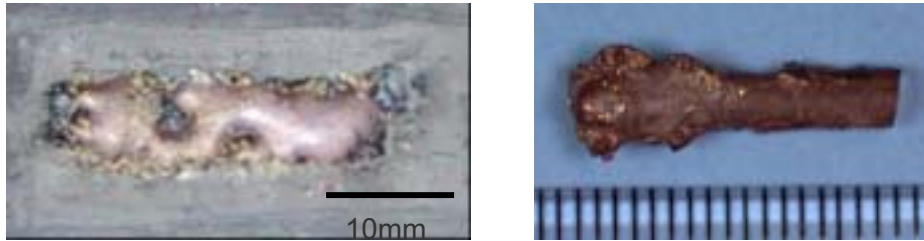
Effects of laser melting conditions on the shape and surface conditions of scan tracks

It is significant to investigate the laser melting conditions, such as laser power, scan speed, traveling speed and so on, in order to fabricate superior laser-melted bodies. Therefore, we investigated the effects of laser power, scan speed and traveling speed on the shape and surface conditions of scan tracks. Figure 3 shows the change in shape of scan track of blended powder with scan speed and traveling speed. In the case of higher power (334 W on the surface), higher scan speed (816 mm/s) and lower traveling speed (0.41 mm/s) as shown in Fig.3(a), the continuity in shape of the laser-melted body is lost and the laser-melted body becomes round in shape during the melting-solidification process. This may be because the powder absorbed too much amount of energy due to higher laser power and lower traveling speed. These conditions create a large and deep melt pool having a surface thermal gradient along both the traveling and scanning directions. This in turn induces a surface tension gradient in the liquid, that favors the formation of surface ripples behind the laser moving front [9]. When the traveling speed is slow, low frequency high amplitude ripples tend to develop which become frozen after solidification. Moreover, a large size melt pool will take longer to solidify and so its surface is exposed to oxygen contamination for longer periods. This surface adsorbed oxygen could also be responsible for the “balling” effect observed by further increasing the surface tension of the liquid.

On the other hand, in the case of lower power (169 W on the surface), lower scan speed (508 mm/s) and higher traveling speed (3.05 mm/s) as shown in Fig.3(b), although fewer “balling” of the surface is observed, the continuity in shape of the body can be obtained and the surface shows to be fairly smooth. In this case, the melt pool is less deep and narrower; a thermal

gradient mainly develops parallel to the traveling speed. The surface tension gradient will now cause ripples to have high frequency and low amplitude, providing a smoother surface. Additionally, solidification occurs at a faster rate on the melt pool and less time is available for surface ripples to fully develop. These ripples are of a high frequency due to the faster traveling speed.

Figure 4 shows the shape of scan track of the MA powder. Comparing with the shape of scan track of the blended powders, although some large pores exist in the body, the surface is smooth and few “balling” are observed. This existence of some large pores may be caused by higher oxygen and carbon contents in the MA powder.



(a) $V_s=816$ mm/s, $V_t=0.41$ mm/s (b) $V_s=508$ mm/s, $V_t=3.05$ mm/s

Fig.3 Change in shape of scan tracks of the blended powder with scan speed and traveling speed



Fig.4 Shape of scan track of the MA powder

Effects of powder characteristics on the microstructure

Figure 5 shows the microstructure of laser-melted body of the blended powder. The microstructure appears to be that of a liquid sintered particles and the size of sintered clusters is different depending on the position in the body. This indicates that partial melting of the blended powder took place. However, at the center the structure is more homogenous, dense and has a cellular structure appearance. This figure corresponds to the microstructure along a vertical direction to the laser traveling speed, that in the horizontal direction to the laser traveling speed was also similar. This fact suggests that the solidification took place rapidly and the concentration gradient of oxygen in liquid state existed in the body as already reported[10]. Figure 6 shows comparison in microstructure of the laser-melted body between the blended powder and the MA powder. The microstructure of the blended powder shows to be that of a liquid sintered particles, while that of the MA powder is a very fine cellular structure. This is caused by difference of powder characteristics between both powders. In Fig.6(a) and Fig.7, the liquid sintered particles of symbol A is primary TiNi and the lamellar structure of symbol B is a eutectic mixture of TiNi and Ti_4Ni_2O as reported by Shugo et al.[10]. Comparing with the microstructure in this reference and Fig.6(a), the oxygen content is estimated at about 0.3 mass%.

In the case of blended powder, the concentration gradient in the liquid alloy results in existence of the lamellar area. The distributions of Ti, Ni, O and C elements were examined by means of a SEM with EDX. Scanning electron micrographs and EDX analyses of the laser-melted bodies of the blended powder and the MA powder are shown in Fig.7 and 8, respectively. In the case of blended powder, the liquid sintered particles and the lamellar structure exist as shown Fig.7(a). The distributions of Ti and Ni elements of the lamellar area (B) are little

different from those of the liquid sintered particles (A) as shown in Fig.7(b) and (c).

On the other hand, in the case of the MA powder, the lamellar area is not observed probably because the MA powder is not only alloy but also amorphous state. In this case, since very small particles were observed in optical microstructure as shown in Fig.6(b), the EDX analysis was carried out. The results of SEM observation and EDX analyses in Fig.8 do not suggest existence of precipitates such as oxides or carbides except the generation of very small pores due to higher oxygen and carbon of the MA powder.

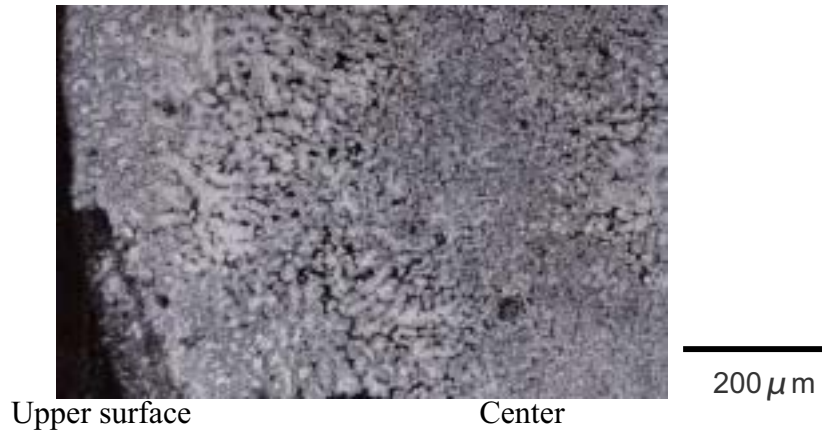


Fig.5 Microstructure of laser-melted body of the blended powder.

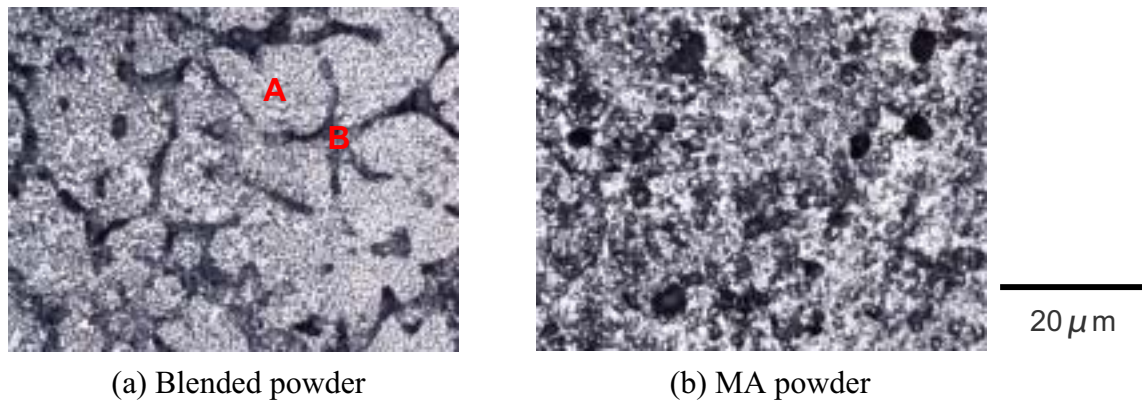


Fig.6 Comparison in microstructure of laser-melted bodies between the blended powder and the MA powder

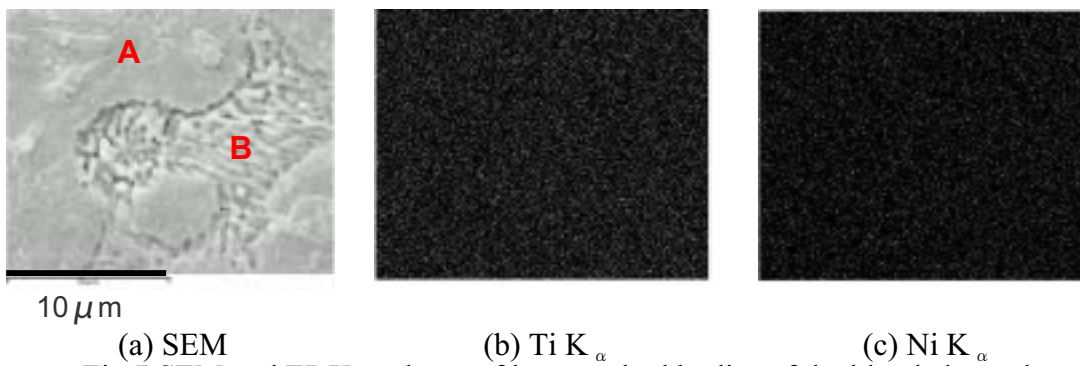


Fig.7 SEM and EDX analyses of laser-melted bodies of the blended powder

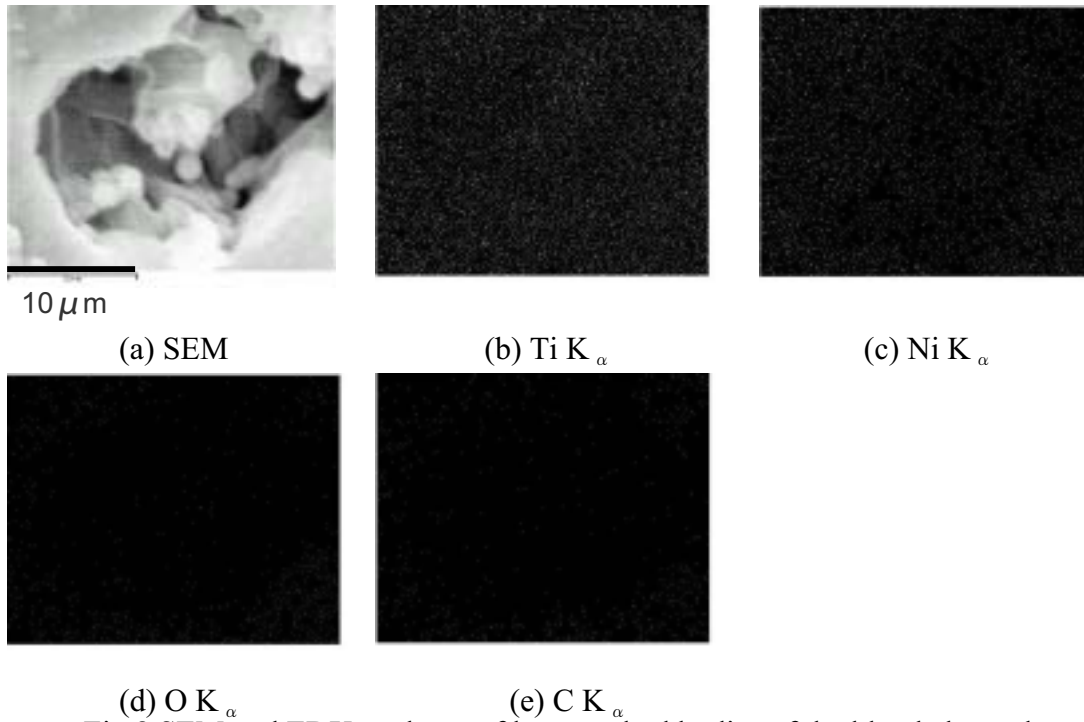


Fig.8 SEM and EDX analyses of laser-melted bodies of the blended powder

Comparing with the microstructure of sintered body by a pulse-current pressure sintering, the microstructure of the laser-melted body is greatly different from that of the sintered body. In the case of the as-sintered body of the blended powder, the microstructure is very inhomogeneous. Therefore, the solid-solution treatment is needed to homogenize the structure for a long time[4-6]. The results of X-ray diffraction patterns of the laser-melted body of the blended powder and the MA powder are given in Fig.9. It is found from this figure that the microstructure of laser-melted body is consisted of homogeneous TiNi phase in every laser-melted conditions. This suggests that the laser-melted body may show the shape memory effect. Since the peak of TiNi phase in the MA powder is higher than that in the blended powder, the microstructure of the former is more homogeneous and dense than that of the latter as shown in Fig.6. In the case of the sintered body, similar results were obtained. Thus, the MA powder results in more homogeneous and dense structure of the laser-melted body.

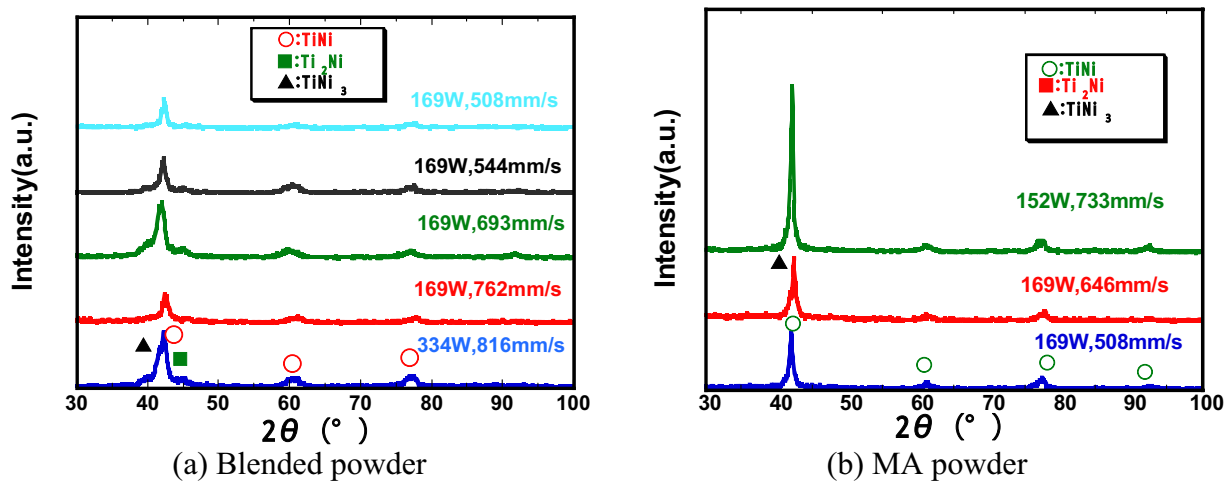


Fig.9 X-ray diffraction patterns of laser-melted bodies of the blended powder and the MA powder

Shape Memory Characteristics

In this study, the existence of the shape memory effect was examined by DSC measurements. The results of laser-melted body of the blended powder and the MA powder are shown in Fig.10. In the case of the blended powder, since the peaks of exothermic and endothermic reactions are observed clearly, this body has the shape memory effect. The martensite peak temperature and the reverse transformation peak temperature are 294 K and 333 K, respectively. The latter is nearly equal to the peak temperature of the wrought material of the same composition, but the former is lower than the peak temperature of the wrought material. On the other hand, in the case of the MA powder, since the peak of both reactions is not clearly observed regardless of homogeneous TiNi phase as described above, the body does not show the shape memory effect. This is because the MA powder contains high oxygen and carbon as already reported in the case of sintered materials [11]. The lower oxygen and carbon of the MA powder resulted in the shape memory effect of the sintered body. Therefore, it is important to use lower oxygen and carbon powder in order to fabricate superior shape memory alloys.

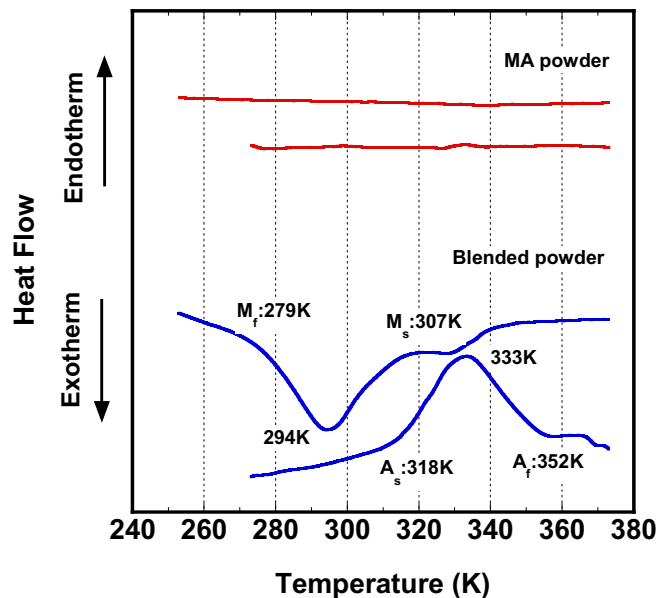


Fig.10 DSC results of laser-melted alloys of the blended powder and the MA powder

Conclusions

In this study, we attempted to fabricate Ti-Ni shape memory alloys by CO₂ laser melting. The laser melting conditions were investigated experimentally, and the microstructure and shape memory characteristics of the laser-melted specimens were also examined. The results obtained are as follows:

- (1) The laser-melted specimens having continuous columnar (i.e., rod-like appearance) shape and smooth surface can be fabricated in both cases of the blended powder and the MA powder at the power of 169 W on the surface, the scan speed of 508 mm/s and the traveling speed of 3.05 mm/s.
- (2) The microstructure of the blended powder resembles that of liquid sintered particles, while that of the MA powder consists of very fine cells. The MA powder results in more homogeneous structure of the laser-melted body than the blended powder. The laser melting blended powder is

less dense than the MA powder.

(3) The laser-melted specimen fabricated from elemental powders exhibited clearly a shape memory effect, but that from MA powder did not exhibit it, although the latter showed more homogeneous and dense microstructure than the former.

References

- [1] J.J. Beaman, J.W. Barlow, D.L. Bourell, R.H. Crawford, H.L. Marcus and K.P. McAlea, *Solid Freeform Fabrication: A New Direction in Manufacturing*, Kluwer Academic Publishers, Massachusetts, 1997.
- [2] D.L. Bourell, H.L. Marcus, J.W. Barlow and J.J. Beaman, "Selective laser sintering of metals and ceramics", *International Journal of Powder Metallurgy*, Vol.28, No.4, 1992, pp.369-381.
- [3] M.K. Agarwala, D.L. Bourell, J.J. Beaman, H.L. Marcus and J.W. Barlow, "Direct selective laser sintering of metals", *Rapid Prototyping Journal*, Vol.1, No.1, 1995, pp.26-36.
- [4] H. Kyogoku, T. Tanbo, M. Yokota, S. Komatsu, F. Yoshida, T. Sakuma and U. Iwata, "Influence of composition on thermo-mechanical properties of TiNi shape memory alloy fabricated by spark-plasma sintering", *Advances in Powder Metallurgy & Particulate Materials-2001*, Part7, Compiled by W.B. Eisen and S. Kassam, MPIF, New Jersey, 2001, pp.1-9.
- [5] T. Watanabe, H. Kyogoku, F. Yoshida and T. Sakuma, "Fabrication of TiNi shape memory alloy by spark-plasma sintering and its thermo-mechanical properties", *Transactions of the Materials Research Society of Japan*, Vol.26, No.1, 2001, pp.149-152.
- [6] H. Kyogoku, F. Yoshida and S. Komatsu, "Shape memory properties of Ti-Ni alloy fabricated by spark-plasma sintering method", *International Journal of Materials Processing Technology (CD-ROM)*, Vol.117, Issue 3, 2001, pp.1-6.
- [7] L.B. Niu, T. Sakuma, H. Takaku, H. Kyogoku, and Y. Sakai, "Erosion resistance of Ti-Ni shape memory alloy to hot water jet", *Materials Science Forum*, Vol.394-395, 2002, pp.353-356.
- [8] L.B. Niu, T. Sakuma, Y. Sakai, H. Kyogoku, and H. Takaku, "Hot water jet erosion characteristics of Ti-Ni shape memory alloys", *Materials Transactions*, Vol.43, No.5, 2002, pp.840-845.
- [9] T.R. Anthony and H.E. Cline, *J. Applied Physics*, Vol. 48, No 9, 3888-3894 (1977).
- [10] Y. Shugo, S. Hanada and T. Honma, "Effect of oxygen content on the martensite transformation and determination of defect structure in Ti-Ni alloys", *Bulletin of research Inst. Mineral Dressing and Metallurgy (Tohoku University)*, Vol.41, 1985, pp.23-34.
- [11] H. Kyogoku, A. Terayama, M. Sakamura and S. Komatsu, "Fabrication of shape memory alloy powder by mechanical alloying", *Proceedings of JSME/ASME International Conference on Materials and Processing 2002*, Vol.1, 2002, pp.136-141.